Ultraviolet Photolysis of HCHO: Absolute HCO Quantum Yields by Direct Detection of the HCO Radical Photoproduct

Paula Gorrotxategi Carbajo, Shona C. Smith, Anne-Louise Holloway, Carina A. Smith, Francis D. Pope,[†] Dudley E. Shallcross, and Andrew J. Orr-Ewing*

School of Chemistry, University of Bristol, Cantock's Close, Bristol, BS8 1TS, United Kingdom

Received: August 7, 2008; Revised Manuscript Received: October 9, 2008

Absolute quantum yields for the radical (H + HCO) channel of HCHO photolysis, Φ_{HCO}, have been measured for the tropospherically relevant range of wavelengths (λ) between 300 and 330 nm. The HCO photoproduct was directly detected by using a custom-built, combined ultra-violet (UV) absorption and cavity ring down (CRD) detection spectrometer. This instrument was previously employed for high-resolution (spectral resolution ~0.0035 nm) measurements of absorption cross-sections of HCHO, $\sigma_{HCHO}(\lambda)$, and relative HCO quantum yields. Absolute Φ_{HCO} values were measured at seven wavelengths, λ = 303.70, 305.13, 308.87, 314.31, 320.67, 325.59, and 329.51 nm, using an independent calibration technique based on the simultaneous UV photolysis of HCHO and Cl_2. These Φ_{HCO} measurements display greater variability as a function of wavelength than the current NASA-JPL recommendations for Φ_{HCO}. The absolute $\Phi_{HCO}(\lambda)$ determinations and previously measured $\sigma_{HCHO}(\lambda)$ were used to scale an extensive set of relative HCO yield measurements. The outcome of this procedure is a full suite of data for the product of the absolute radical quantum yield and HCHO absorption cross-section, $\Phi_{HCO}(\lambda)\sigma_{HCHO}(\lambda)$, at wavelengths from 302.6 to 331.0 nm with a wavelength resolution of 0.005 nm. This product of photochemical parameters is combined with high-resolution solar photon flux data to calculate the integrated photolysis rate of HCHO to the radical (H + HCO) channel, J(HCO). Comparison with the latest NASA-JPL recommendations, reported at 1 nm wavelength resolution, suggests an increased J(HCO) of 25% at 0° solar zenith angle (SZA) increasing to 33% at high SZA (80°). The differences in the calculated photolysis rate compared with the current HCHO data arise, in part, from the higher wavelength resolution of the current data set and highlight the importance of using high-resolution spectroscopic techniques to achieve a complete and accurate picture of HCHO photodissociation processes. All experimental $\Phi_{HCO}(\lambda)\sigma_{HCHO}(\lambda)$ data are available for the wavelength range 302.6−331.0 nm (at 294 and 245 K and under 200 Torr of N_2 bath gas) as Supporting Information with wavelength resolutions of 0.005, 0.1, and 1.0 nm. Equivalent data sets of $\Phi_{H_2+CO}(\lambda)\sigma_{HCHO}(\lambda)$ for the molecular (H_2 + CO) photofragmentation channel, produced using the measured $\Phi_{HCO}(\lambda)$ $\sigma_{HCHO}(\tau)$ values, are also provided at 0.1 and 1.0 nm resolution.

1. Introduction

Formaldehyde (HCHO) is ubiquitous in the troposphere, being an intermediate product in the hydroxyl (OH) radical initiated oxidation of methane and higher hydrocarbons, as well as a primary emission component from fossil fuel and biomass burning. With a relatively long atmospheric lifetime of the order of a few hours,[1] and typical concentrations ranging from ~0.2 ppbv (parts per billion by volume) in the background troposphere[2] up to tens of ppbv in polluted urban locations,[3,4] HCHO has the potential to influence significantly both local and regional scale atmospheric chemistry.

The two major removal processes for atmospheric HCHO are photolysis by sunlight for λ < 361 nm[5] and reaction with OH radicals ($k_{OH+HCHO} = (8.5 \pm 1.2) \times 10^{-12}$ molecule^{-1} cm^3 s^{-1} T = 294 K).[1] The principal HCHO loss mechanism in the troposphere is photodissociation, which occurs via two major pathways, a molecular (eq 1) and a radical (eq 2) forming channel, with threshold wavelengths indicated in parentheses:

$$HCHO + h\nu \rightarrow H_2 + CO \quad (\lambda < 361 \text{ nm}) \qquad (1)$$

$$HCHO + h\nu \rightarrow H + HCO \quad (\lambda < 330 \text{ nm}) \qquad (2)$$

The radical channel photoproducts, H and HCO, react with atmospheric O_2 producing hydroperoxy (HO_2) radicals which are recycled to OH radicals through reaction with O_3 or NO. The photolysis of NO_2 produced by the latter process leads to production of O_3, a key component of photochemical smog. Through the indirect production of HO_x (=OH + HO_2), HCHO can influence the oxidizing capacity of the atmosphere, because OH is the principal daytime tropospheric oxidant. As a consequence of its relatively long atmospheric lifetime, HCHO acts as a HO_x reservoir species, influencing the spatial distribution of HO_x radicals. Recent ground-based HO_x field measurements in polluted environments illustrated that HCHO photolysis can be a more significant radical source in the early morning and late evening than the primary OH production route of O_3 photolysis followed by reaction of the resultant O(^{1}D) with H_2O.[6−8] This HO_x production rate by HCHO photolysis is favored because the longer wavelength threshold for the channel 2 pathway of HCHO photolysis, compared to that for O_3 photolysis, results in greater rates of HCHO photolysis at high solar zenith angles (SZA).

As HCHO is such a key and influential atmospheric constituent, its photochemistry must be well understood and correctly

* Corresponding author. E-mail: a.orr-ewing@bristol.ac.uk. Fax:+44 117 925 0612. Phone:+44 117 928 7672.

[†] Current address: Centre for Atmospheric Sciences, Department of Chemistry, University of Cambridge, Lensfield Road, Cambridge, CB2 1EW, UK.

10.1021/jp8070508 CCC: $40.75 © 2008 American Chemical Society
Published on Web 11/11/2008

quantified in atmospheric models. Simulations which include the radical channel for HCHO photolysis therefore require accurate values of wavelength-dependent HCHO absorption cross-sections, $\sigma_{HCHO}(\lambda)$, and absolute HCO quantum yields, $\Phi_{HCO}(\lambda)$, to combine with solar flux data to calculate the photolysis rates of HCHO via the radical channel, J(HCO). There have thus been numerous detailed prior experimental and theoretical studies of HCHO photodissociation.[9−19]

Several investigations of the wavelength, pressure, and temperature dependence of σ_{HCHO} have been carried out at near-UV wavelengths and the current recommendations of Sander et al.[1] are the measurements of Meller and Moortgat[17] obtained at a spectral resolution of ∼0.025 nm. More recent measurements from our laboratory were obtained with a spectral resolution of 0.0035 nm, and showed that the peak σ_{HCHO} values in the wavelength range 300−340 nm are significantly higher than had been measured previously with lower resolution spectrometers.[20−22] These findings were recently confirmed experimentally by Gratien et al.[23,24] The temperature dependence of the HCHO absorption cross-sections has also been studied by a number of groups,[17,20−22,25] and these data and recent spectral simulations[22] showed that at reduced temperatures the peak intensities at the maxima of each absorption band are greater.

Moortgat and Warneck[14] published one of the most comprehensive studies of HCHO photodissociation and provided a detailed review of early measurements of the quantum yields for the photoproducts. The experiments of Moortgat and Warneck[14] employed the detection of CO and H_2 and provided reliable determination of absolute quantum yields for the two channels of HCHO photolysis (1 and 2). Further measurements of the wavelength and pressure dependence of HCHO photooxidation in a number of different gases (CO_2, NO, air, and HCHO) indicated that studies carried out at reduced pressures could be used to describe HCHO photochemistry in the atmosphere for $\lambda < 355$ nm, with collisional quenching effects found to be negligible even in 1 atm of air. A subsequent study by Moortgat et al.[15] illustrated that measurements of HCHO photoproduct yields carried out at a reduced temperature of 220 K were not significantly different from those made at 294 K in the 300−330 nm wavelength range.

In the most recent study of quantum yields from HCHO photolysis, Smith et al.[18] measured the radical products indirectly using chemical amplification with NO, and subsequent detection of NO_2 by chemical ionization mass spectroscopy (CIMS). The instrument wavelength resolution for the relative radical quantum yield and HCHO absorption cross-section measurements was ±0.62 nm at fwhm (full width at half-maximum height). The measured relative quantum yields for HCO/H were normalized to a single wavelength quantum yield value of 0.753 at a photolysis wavelength of 303.75 nm based on the recommendations of DeMore et al.[26] The results of Smith et al.[18] illustrated greater wavelength dependence in the radical quantum yields for HCHO photolysis than had previously been observed, providing evidence for the importance of competition between dissociation pathways in HCHO via internal conversion from the photoexcited $\tilde{A}^1A_2$ (S_1) state to the $\tilde{X}^1A_1$ (S_0) state or intersystem crossing to the $\tilde{a}^3A_2$ (T_1) state.[16] These results highlighted the importance of high-resolution measurements to provide accurate characterization of such complicated photodynamic processes.

The current recommendations of Sander et al.[1] for both HCHO absorption cross-sections and photolysis quantum yields are provided with a maximum wavelength resolution of 1 nm. The recommendations for HCO quantum yields from channel 2 are based on fitting data sets from the following studies: Lewis et al.,[9] Horowitz et al.,[11] Clark et al.,[12] and Tang et al.,[13] who used radical scavenger methods; Marling et al.,[10] who detected H_2, HD, and D_2 following HDCO photolysis; Moortgat et al.,[15] who made measurements of H_2 and CO yields; and Smith et al.,[18] who scaled relative HCO/H yields to a single wavelength value recommended by DeMore et al.[26] As such, the current recommendations for the radical quantum yields from HCHO photolysis are based on indirect measurements of the radical photoproducts and provide insufficient wavelength resolution to capture the likely variation in the HCO quantum yields. This paper presents the first high-resolution absolute HCO quantum yields for the UV photolysis of HCHO, measured by direct detection of the HCO photoproduct using absorption spectroscopy. The measurements employed a custom-built UV absorption and cavity ring down (CRD) spectrometer previously used to obtain *relative* HCO yields and absorption cross-sections of HCHO in the $\tilde{A}^1A_2-\tilde{X}^1A_1$ electronic band at high resolution over the range of tropospherically relevant wavelengths from 300 to 340 nm.[20−22] The current work draws to a conclusion the extensive high-resolution spectroscopic measurements of HCHO carried out in our laboratory over recent years.

2. Experimental Section

2.1. Apparatus. The apparatus and methodology used in these investigations has previously been described by Pope et al.[20,21] and Smith et al.[22] and was subject to only minor modification for the current studies. The spectrometer consisted of a 600 (l) × 300 (w) × 200 (h) mm stainless steel chamber fitted with separate gas inlets for addition of HCHO and Cl_2 and two gas outlets. The first outlet allowed rough evacuation of the chamber using a rotary pump, and the second allowed evacuation to low base pressures by a turbomolecular pump backed by a rotary pump. The chamber was fitted with two calibrated capacitance manometers (0−10 and 0−1000 Torr) to measure the partial pressures of reactants and bath gas added to the chamber. Flanges allowed feedthrough of two type-K thermocouples to monitor the internal temperature of the chamber. Coolant output from a chiller circulator could be flowed through a loop of copper piping located inside the chamber for measurements at reduced temperatures. Synthesis and purification of HCHO was carried out using the method of Spence and Wild[27] and subsequently described by Pope et al. and Smith et al.[20−22] The resultant liquid HCHO held in a cold trap was then either admitted directly into the ring-down chamber by warming or diluted in a 5 L glass bulb with oxygen-free N_2 (OFN, 99.998%) to give typical dilutions of ∼10% HCHO in N_2, with a minimum dilution of 20%. Formaldehyde bulbs were prepared at least once daily to avoid contamination of the gas by polymerization of HCHO.

On the long axis of the spectrometer, a CRDS system was implemented to measure the relative concentration of HCO radicals. For most measurements reported here, HCO was probed 10 μs after HCHO photolysis using the diffuse (0,8,0)−(0,0,0) vibrational band of the $\tilde{A}^2A''-\tilde{X}^2A'$ electronic transition at $\lambda = 645$ nm. The time delay between the photolysis and probe lasers allowed thermalization of any internal excitation of the photolytically produced HCO prior to detection. For a small number of determinations of temporal decays of HCO concentrations (described in section 2.5) the time delay was varied from 0 to 80 μs. The CRDS probe beam was produced using the third harmonic output of a pulsed Nd:YAG laser (Inlite II-20, Continuum Inlite), with a pulse repetition frequency of

10 Hz and output powers of ~50 mJ pulse^{-1}, to pump a dye laser (Cobra, Sirah) circulating a solution of DCM (4-dicyanomethylene-2-methyl-6-(*p*(dimethylamino)styryl)-4*H*-pyran) laser dye in methanol. The manufacturer specified bandwidth of the CRDS probe beam was 0.08 cm^{-1} at 570 nm and typical visible light output powers were between 0.6 and 2.0 mJ pulse^{-1}. The probe beam was spatially filtered using a pinhole and focused into the chamber through the first of two high-reflectivity, plano-concave mirrors with a radius of curvature of 1 m, giving a TEM_{00} beam diameter of ~0.6 mm in the center of the cavity. The exponential decay of light leaking out of the second high-reflectivity mirror was monitored by a photomultiplier tube (PMT, Electron Tubes 9128B). The PMT signal was amplified and then digitized by an oscilloscope (LeCroy 6030). Following internal averaging of 20 shots by the oscilloscope, the CRDS signal was analyzed using a fast Fourier transform (FFT) method[28] on the portion of the waveform containing the single exponential ring-down decay. Typical background ring-down times (RDTs) were ~11 μs. Data accumulation and analysis were carried out using a custom written LabView program.[29]

The UV photolysis beam was produced using the frequency doubled output of a dye laser (Cobra Stretch, Sirah), circulating either DCM (λ = 628−642 nm), a mixture of DCM and LDS 698 (Pyridine 1) (λ = 650−660 nm), or Sulfurhodamine (λ = 606−618 nm) dye, pumped by the second harmonic of a Nd:YAG laser (Continuum Surelite III) at a pulse repetition frequency of 10 Hz. Frequency doubling of the visible output of the dye laser was achieved using a KDP (Potassium Dihydrogen Phosphate) crystal. Typical UV energy prior to the ring-down chamber was 0.8 mJ pulse^{-1} and was maintained above 0.6 mJ pulse^{-1} and below 1 mJ pulse^{-1} for all of the experiments. The UV beam had a circular profile with a diameter of 0.9 mm (in the center of the ring-down chamber) and a measured bandwidth of 0.35 cm^{-1} (0.0035 nm).[22] The photolysis wavelength was determined by monitoring a fraction of the visible output from the dye laser with a wavemeter (Coherent Wavemaster, range 400−1095 nm, resolution 0.002 nm, accuracy ±0.005 nm). Prior to the chamber, a small fraction of the photolysis beam was reflected onto a fast photodiode to monitor the initial UV light intensity. The photolysis laser beam then entered the chamber at one end of the long axis through a UV grade fused silica wedged window, and was turned through 90° by a right-angled prism mounted inside the vacuum chamber to overlap the probe beam for ≤10 cm at a shallow angle of ~3°. Losses of UV beam intensity after passing through the window and prisms led to typical energies of ~0.55 mJ pulse^{-1} in the center of the ring-down chamber. At the opposite end of the chamber the photolysis beam was again turned through 90° by a prism to exit the chamber through a wedged fused silica window, and was directed onto the face of a second fast photodiode to monitor the UV light intensity exiting the chamber. The change in the UV light intensity allowed determination of σ_{HCHO} values while the CRDS data were analyzed to obtain relative HCO absorption coefficients, α_{HCO}^{rel} (see below), with both parameters evaluated as a function of UV excitation wavelength.

2.2. Methodology. The photolysis rate coefficient for the HCHO radical-forming channel, J(HCO), can be calculated by using eq 3:

$$J(\mathrm{HCO}) = \int_{\lambda_1}^{\lambda_2} F(\lambda)\sigma_{\mathrm{HCHO}}(\lambda)\Phi_{\mathrm{HCO}}(\lambda)\,\mathrm{d}\lambda \qquad (3)$$

where $F(\lambda)$ is the spherically integrated solar photon flux, $\sigma_{HCHO}(\lambda)$ is the HCHO absorption cross-section, and $\Phi_{HCO}(\lambda)$ is the absolute quantum yield of HCO radicals. These three parameters all depend on the excitation (UV) wavelength, λ. Thus, the rate of photolytic formation of HCO radicals at a given single wavelength is given by eq 4:

$$\frac{\mathrm{d[HCO]}}{\mathrm{d}t} = [\mathrm{HCHO}]\sigma_{\mathrm{HCHO}}(\lambda)\Phi_{\mathrm{HCO}}(\lambda)F(\lambda) \qquad (4)$$

The investigations presented here employed a custom-built CRDS setup,[21] as described in the previous section, to measure directly relative yields of HCO radicals produced by the UV photolysis of a dilute gaseous sample of HCHO. Under the conditions of our experiments, the concentration of HCHO was held constant, and the excitation laser delivered pulses of a well-defined duration, giving conditions of constant UV flux if data were normalized by laser pulse energy to divide out the effects of small pulse-to-pulse variations. The amount of HCO formed at a constant time after each UV laser pulse at a fixed wavelength was thus proportional to the product of $\sigma_{HCHO}(\lambda)$ and $\Phi_{HCO}(\lambda)$.

The CRDS experiments, however, measure the product of the absorption coefficients for HCO ($\alpha_{HCO}(\lambda) = \sigma_{HCO}(\lambda)$[HCO]) and the distance (d) over which the HCO is formed (at a given UV excitation wavelength). Conversion from CRDS data to absolute concentrations of HCO radicals thus requires knowledge of d and the absorption cross-section for HCO (σ_{HCO}) at the wavelength of the probe laser. The former parameter is determined by the region of overlap of the photolysis and probe laser beams and their spatial intensity profiles and was not precisely known in the experiments. A value of the HCO absorption cross-section has been determined for the sharply structured $\tilde{A}^2A''-\tilde{X}^2A'$ (0,9,0)−(0,0,0) band,[30] but not for the diffuse (0,8,0)−(0,0,0) band that was employed in the current study to avoid any effects of laser line width on the retrieval of absorption coefficient data.[31] Measurement of HCO absorption via the (0,9,0)−(0,0,0) band and determination of HCO concentrations is one possible option for deriving absolute quantum yields, but the uncertainties in the absorption path length and the HCO cross-section would propagate unfavorably into the final quantum yield values. We thus preferred an alternative strategy to provide absolute quantum yield data based on scaling factors resulting from production of HCO by two competing photolytic processes; this method does not require precise knowledge of either d or σ_{HCO}. The calibration procedure is described later, and was performed at seven selected UV wavelengths. Relative yields of HCO, measured at high wavelength resolution across the UV band system of HCHO,[21,32] were then scaled to absolute values using the seven calibration points. The strategy for determining the wavelength-dependent *relative* yields of HCO is outlined first, and is followed by a description of the calibration method to derive *absolute* values.

The cavity RDT, τ, is the time taken for the probe light injected into the ring-down cavity to decay to 1/e of its initial intensity (as monitored by a detector located behind one cavity mirror).[33] In the presence and absence of the HCO, the RDTs are denoted respectively as τ and τ_0 and their reciprocals (k and k_0) are the rate coefficients for the decay of light intensity. The change in the ring-down rate coefficient (Δk) on photolytic production of HCO is related to the HCO absorption coefficient by eq 5:

$$\alpha_{\mathrm{HCO}}(\lambda) = \frac{\Delta kL}{cd} \qquad (5)$$

where c is the speed of light, L is the separation of the mirrors in the ring-down experiment, and d, as mentioned above, is the

distance of overlap of the probe laser with the region of formation of HCO radicals. Equation 5 implicitly assumes a uniform spatial distribution of HCO radicals over this distance. The value of d may change with realignment of the photolysis and probe lasers, but under the conditions of any particular set of measurements, d and L take constant values. By ensuring partial overlap in the scanned HCHO photolysis wavelength ranges for all data sets for HCO yield measurements, effects of variation in the value d are eliminated. We can thus define a relative yield (in arbitrary units) of HCO radicals at any UV laser excitation wavelength, $\alpha_{HCO}^{rel}(\lambda)$, that is normalized to the UV laser pulse energy, P_{UV}, and the (carefully regulated) concentration of HCHO in the chamber, as:

$$\alpha_{HCO}^{rel}(\lambda) = \frac{\Delta k}{P_{UV}[HCHO]} \propto \sigma_{HCHO}(\lambda)\Phi_{HCO}(\lambda) \qquad (6)$$

As is indicated in eq 6, this measured $\alpha_{HCO}^{rel}(\lambda)$ at any particular photolysis wavelength is proportional to the product of the HCHO absorption cross-section and the absolute HCO quantum yield at the photolysis wavelength, and can thus be scaled by a constant proportionality factor to give absolute values of the product of $\sigma_{HCHO}(\lambda)$ and $\Phi_{HCO}(\lambda)$ at all UV excitation wavelengths, as discussed further in section 3.4.

The initial part of this study concentrated on determining the wavelength dependence of the relative HCO yields from HCHO photolysis by measuring a high-resolution photofragment excitation (PHOFEX) spectrum of HCO simultaneously with HCHO absorption cross-sections[20−22,32] (see section 2.3) over the UV photolysis wavelength range from 302.6 to 331.0 nm. The relative HCO yields, as discussed above, are proportional to the product of $\sigma_{HCHO}(\lambda)$ and $\Phi_{HCO}(\lambda)$, but the constant of proportionality required to put data on an absolute scale is unknown for our apparatus. Further investigations thus determined a number of single-wavelength *absolute* HCO quantum yield values using an independent calibration technique (see section 2.4). These single-wavelength absolute HCO quantum yields were then combined with the initial $\alpha_{HCO}^{rel}(\lambda)$ and $\sigma_{HCHO}(\lambda)$ measurements to produce a full set of data at high wavelength resolution for the absolute product $\sigma_{HCHO}(\lambda)\ \Phi_{HCO}(\lambda)$ in the interval $\lambda = 302.6-331.0$ nm. The resultant laboratory data are appropriate for use with solar flux data at the same resolution to calculate the rate of photolysis of HCHO via the radical channel, J(HCO), using eq 3. The high wavelength resolution enables accurate evaluation of the effect of binning experimental and solar flux data into larger wavelength intervals for the purpose of inclusion in models.

2.3. Relative HCO Yields. Measurement of high spectral resolution (~0.0035 nm) *relative* HCO absorption coefficients (α_{HCO}^{rel})for the tropospherically relevant wavelength range from 302.6 to 331.0 nm followed the procedure described previously by Pope et al.[21] for measurements over the more limited wavelength region from 313 to 320 nm. UV wavelength scans were performed using a static sample of 1 Torr of gaseous pure HCHO inside the vacuum chamber, and relative HCO yields were determined by CRDS at a fixed probe laser wavelength. (Validation experiments under the conditions of HCHO partial pressure and low laser pulse energy (<1 mJ per pulse) employed demonstrated no measurable loss of HCHO or buildup of photoproducts for such static samples within a measurement period of 30 min.) An additional 100 or 200 Torr of N_2 (OFN) was added to the chamber to ensure all of the HCO radicals produced by the photolysis of HCHO were vibrationally relaxed and rotationally thermalized, so that detection by CRDS was not subject to any HCO quantum state population bias resulting from the dissociation dynamics.[5,34] Detailed investigations showed that 100 Torr of N_2 bath gas was sufficient to thermalize any HCO radicals formed in internally excited states following UV photolysis at wavelengths between 316 and 320 nm, but most experiments were conducted at 200 Torr of N_2 to err on the side of caution.

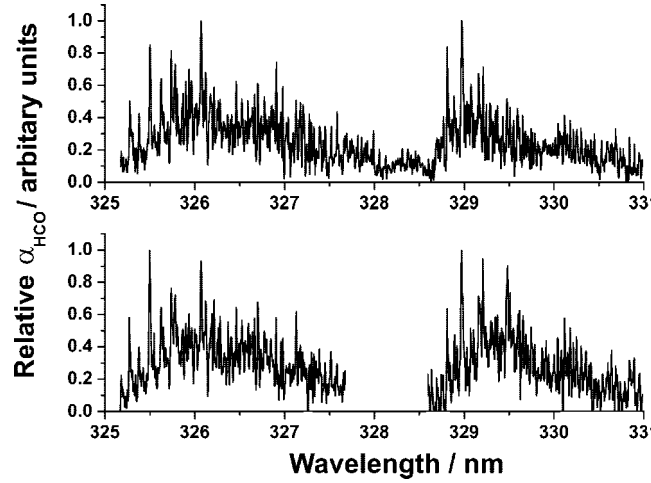

Figure 1. Relative HCO absorption coefficients, α_{HCO}^{rel}, measured at 294 K with 0 (bottom panel) and 200 Torr (top panel) N_2 bath gas. Data are shown at a wavelength resolution of 0.005 nm for the range 325.170−330.985 nm; the UV photolysis wavelength in this region is insufficiently energetic for photolytic production of vibrationally excited HCO ($\lambda \leq 318$ nm).[34,41] The α_{HCO}^{rel} data are arbitrarily scaled to maximum values of 1 for each plot.

Single PHOFEX scans covering a 0.7 nm UV wavelength interval were recorded, and the HCHO sample was then refreshed before scanning the next interval. Wavelength scans were overlapped by 0.1 nm, and each region was typically recorded two or three times to check reproducibility and to allow averaging of data. Background cavity loss scans over each 0.7 nm UV region were performed in the absence of HCHO, but under otherwise identical experimental conditions of temperature and bath gas pressure both prior and subsequent to each absorption scan. Relative HCO absorption coefficients were calculated with eq 6, with normalization to the concentration of HCHO and the UV laser intensity measured prior to entry to the ring-down chamber. Figure 1 shows an example of the measured α_{HCO}^{rel} data in the wavelength interval 325.170−330.985 nm taken at 294 K, both in the absence of N_2 bath gas and under the typical experimental conditions of 200 Torr of N_2. These α_{HCO}^{rel} values are indicative of the wavelength-dependent variability in the product of the HCHO absorption cross-section and the absolute HCO quantum yield. In principle, the α_{HCO}^{rel} values can be divided by the HCHO absorption cross-sections (reported previously[20,22]) to provide relative quantum yields for HCO production. This procedure has not been applied to these data, however, as it introduces significant noise and large uncertainties into the resultant Φ_{HCO} data from the combined variability and uncertainties in the α_{HCO}^{rel} and σ_{HCHO} values, which are most pronounced in regions of weak absorption (i.e., small σ_{HCHO}).

2.4. Absolute HCO Quantum Yield Measurements. The second part of the investigation entailed measurement of a number of absolute HCO quantum yield values at selected single UV wavelengths using an independent calibration method based on the UV photolysis of Cl_2 in the presence of HCHO, as previously employed by Chen and Zhu,[35] Zhu et al.,[36] and Wang[37] in studies of the UV photolysis of glyoxal, $(CHO)_2$. On simultaneous addition to the ring-down chamber, both

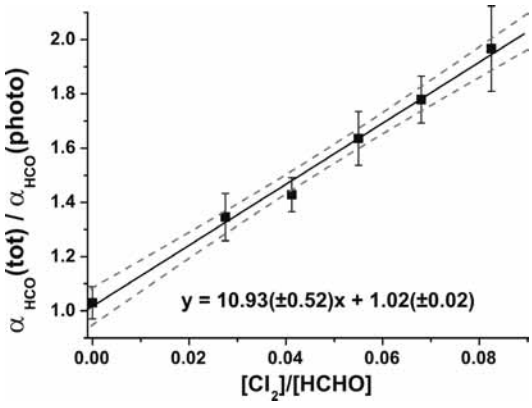

Figure 2. Experimental calibration plot measured at $\lambda = 314.31$ nm from which $\Phi_{HCO} = 0.69 \pm 0.06$ is derived. The data are plotted in the form of eq 9 and analyzed by using the kinetic model based on the data shown in Table 1. The linear regression (solid line) is weighted to the error bars which are ± the precision (1 SD) of the measured $\alpha_{HCO}(tot)/\alpha_{HCO}(photo)$. The outer dashed lines represent the 95% confidence interval.

HCHO and Cl_2 were photolyzed by the UV beam, initiating a chain of photochemical reactions. Cl_2 was photolyzed with a quantum yield of $\Phi_{Cl} = 2$,[38] producing Cl atoms which reacted with HCHO (with a rate constant $k_{HCHO+Cl} = 7.30(+1.10/-0.95) \times 10^{-11}$ molecule^{-1} cm^3 s^{-1} [ref 1]) forming an additional source of HCO radicals:

$$Cl_2 + h\nu \rightarrow 2Cl \quad (7)$$

$$HCHO + Cl \rightarrow HCO + HCl \quad (8)$$

Varying the concentration of Cl_2 added to the ring-down chamber resulted in a change in the concentrations of HCO radicals and therefore the HCO absorption coefficient. HCO absorption coefficients were measured in the presence of HCHO only, denoted as $\alpha^{rel}_{HCO}(photo)$, and in the presence of both HCHO and Cl_2 at different concentrations, $\alpha^{rel}_{HCO}(tot)$. A simple kinetic analysis of the reaction schemes 1, 2, 7, and 8 suggests that the absolute HCO quantum yield can be obtained through the linear relationship, eq 9, which is independent of the volume or pulse energy of the photolysis laser beam:

$$\frac{[HCO]_{tot}}{[HCO]_{photo}} \cong \frac{\alpha^{rel}_{HCO}(tot)}{\alpha^{rel}_{HCO}(photo)} = \frac{\Phi_{Cl}\sigma_{Cl_2}}{\Phi_{HCO}\sigma_{HCHO}}\frac{[Cl_2]}{[HCHO]} + 1 \quad (9)$$

Calibration data produced at seven selected wavelengths between 300 and 330 nm were plotted in the form of eq 9 (i.e., the ratio $\alpha^{rel}_{HCO}(tot)/\alpha^{rel}_{HCO}(photo)$ versus $[Cl_2]/[HCHO]$), and an example taken at a photolysis wavelength of 314.31 nm is shown in Figure 2. The gradients of these calibration plots could, in principle, be used to determine absolute quantum yields for HCO radicals, because the parameters Φ_{Cl} and σ_{Cl_2} (the Cl_2 absorption cross-section) in eq 9 are well-known and constant for a specific single wavelength.[38,39] The HCHO absorption cross-sections required for analysis using eq 9 were previously measured in our laboratory at high wavelength resolution, using the experimental setup described above and under identical experimental conditions.[20,22] Although the experimental plots are observed to be linear, kinetic modeling shows that direct substitution of the gradient of the experimental calibration plot into eq 9 leads to inaccurate values of Φ_{HCO}. The errors arise because of the overly simplistic treatment of the reaction scheme, which includes only reactions 1, 2, 7, and 8, and thus does not take into account side reactions of the reactants and photoproducts. Consequently, an extended kinetic model was implemented using the ACUCHEM program[40] to model the chemistry occurring in the ring-down chamber. This model and the determination of Φ_{HCO} values are described in detail in section 2.5; as we explain later, however, plotting the data in the form of Figure 2, but with a more thorough interpretation of the gradient of the best-fit line than is afforded by eq 9, proves very useful in deducing the true Φ_{HCO} values.

The experimental procedure for producing a calibration plot of $\alpha^{rel}_{HCO}(tot)/\alpha^{rel}_{HCO}(photo)$ versus $[Cl_2]/[HCHO]$ at a single wavelength, such as shown in Figure 2, was as follows. First, an absorption feature near the head of a vibronic band of HCHO was identified by scanning the absorption spectrum over a small UV wavelength region. A UV excitation wavelength was then selected at which the peak in the HCHO absorption cross-section was relatively broad (>0.5 cm^{-1}) so that any small drifts in UV laser wavelength would not result in a large change in the concentration of HCO radicals produced by photolysis of HCHO. The UV photolysis laser was then fixed at the selected wavelength throughout the data acquisition, and the σ_{HCHO} used in later data analysis were taken from the values measured under identical conditions of temperature and pressure in our laboratory.[22]

The next step in the experimental procedure was the measurement of HCO absorption coefficients in the presence of HCHO and with addition of Cl_2. Background RDTs (typically 11.0−11.5 μs) were determined over 50 data points (1 data point being the average of 20 laser shots at a pulse repetition frequency of 10 Hz) with the chamber filled to a partial pressure of 100−200 Torr of N_2 under static gas conditions to account for baseline cavity loss levels (including Rayleigh scattering). The pressure of N_2 bath gas used depended to some extent upon the UV photolysis wavelength because the threshold for formation of vibrationally excited HCO is ~318 nm,[34,41] and this vibrational excitation must be quenched prior to HCO measurements. The ring-down chamber was then evacuated and refilled to a partial pressure equivalent to 1 Torr of HCHO from a bulb of 10−20% pure HCHO diluted in N_2. An additional 100 or 200 Torr of N_2 was added to the chamber. Flow conditions were set up by flowing the HCHO/N_2 mixture from the bulb at a rate of 10 sccm (standard cubic centimeters per minute) and N_2 at a rate of 50 sccm through two calibrated mass flow controllers (MFC) (MKS instruments, 500 and 50 sccm, respectively), and a constant chamber pressure was maintained by partially opening a 1/4 in. Swagelok tap used to throttle the turbomolecular/rotary pumping system. The UV laser beam was then allowed to enter the chamber and the resultant reduced RDT (typically ~10.6−10.9 μs) was recorded for 50 data points.

The final measurement was the determination of the RDT on simultaneous addition of HCHO and Cl_2 to the ring-down chamber. The evacuated chamber was filled with a partial pressure of Cl_2 between 0.027 and 0.082 Torr from a bulb of pure Cl_2 diluted to 5.5% in Argon ($[Cl_2] = 9 \times 10^{14}$ to 3×10^{15} molecule cm^{-3}); 1 Torr of HCHO and 100−200 Torr of N_2 were also added and flow conditions were established as above. The Cl_2/Ar mixture was flowed at a rate of 3.3 sccm from a 10 sccm calibrated MFC (MKS Instruments) to maintain ratios of Cl_2 to HCHO of less than 0.1. The resultant reduced RDT (typically in the range 9.3−10.5 μs) was recorded for 50 data points. All of these procedures were repeated at least ten times for each Cl_2 concentration to allow averaging, with sets of measurements made for five different Cl_2 concentrations. Low concentrations of Cl_2 were employed during calibrations to

TABLE 1: Rate Constants and the ±1 SD Uncertainties Used in the Kinetic Model for Simulating the Time Dependent Decay of HCO Radicals during Calibrations in Which HCHO and Cl_2 Were Simultaneously Added to the Ring-down Chamber

reaction no.	reaction	rate constant/ molecule^{-1} cm^3 s^{-1}	+ uncertainty/ molecule^{-1}cm^{3}s^{-1}	− uncertainty/ molecule^{-1}cm^{3}s^{-1}	ref
R1	HCO + HCO → HCHO + CO	5.00×10^{-11}	4.98×10^{-11}	2.49×10^{-11}	51
R2	HCO + H → H_2 + CO	1.50×10^{-10}	1.49×10^{-10}	0.75×10^{-10}	51
R3	HCHO + H → H_2 + HCO	5.93×10^{-14}	1.54×10^{-14}	1.22×10^{-14}	51
R4	HCHO + Cl → HCO + HCl	7.30×10^{-11}	1.10×10^{-11}	0.95×10^{-11}	1
R5	[a]HCO + Cl → HCl + CO	3.00×10^{-10}	1.20×10^{-10}	1.20×10^{-10}	50
R6	HCO + Cl_2 → HClCO + Cl	7.60×10^{-12}	7.00×10^{-13}	7.00×10^{-13}	52
R7	H + Cl_2 → HCl + Cl	2.19×10^{-11}	3.20×10^{-12}	3.20×10^{-12}	53
R8[b]	HCO → diffusion	1.00×10^3 (s^{-1})			42

[a] The rate constant for reaction 5 has been estimated from a measurement of the Br + HCO reaction rate by Pouletet al.[50] [b] Reaction 8 is an estimation of the effects of diffusion of HCO radicals out of the probe volume with units of s^{-1}.

minimize unwanted side reactions of the photolytically produced Cl atoms, and in particular the rapid reaction between Cl and HCO. Under the chosen conditions, absorption of the probe laser beam (λ = 645 nm) by Cl_2 was negligible. The resultant calibration data were plotted in the form of Figure 2 and analyzed using the extended kinetic model, as described in section 2.5, to obtain each single wavelength Φ_{HCO} value.

2.5. Analysis of Data To Obtain Absolute Φ_{HCO}. As was discussed in section 2.2, probing nascent HCO radicals with the CRDS setup described in section 2.1 does not result in an absolute determination of radical quantum yields from HCHO photolysis, because only relative α_{HCO} values are measured. To determine absolute Φ_{HCO} data, we used the independent calibration method described in section 2.4 and based on relative rates of HCO production photolytically and from reaction of Cl atoms with HCHO. Plots of the experimental data in the form of Figure 2 proved to be linear under our experimental conditions, but simple analysis by direct substitution of the gradients of best-fit lines into eq 9 did not yield accurate Φ_{HCO} values because of the overly simplified chemical scheme on which this equation is based. A more complete kinetic model was therefore developed and numerically integrated using ACUCHEM to simulate the time-dependent evolution of the concentration of HCO radicals in the ring-down chamber. The model accounted for likely side reactions of the reactants and photoproducts and, combined with an analysis of experimental and simulated data plotted in the form of Figure 2, provides the basis for our determinations of Φ_{HCO} values.

The reactions and rate constants shown in Table 1 were incorporated into the model to improve the description of the kinetics following UV laser photolysis of the HCHO/Cl_2/N_2 mixtures. Reaction R8 in Table 1 represents an approximate upper limit for diffusion of HCO radicals out of the probe laser volume. The diffusion rate constant, k_d, is obtained from the report by Reilly et al.[42] of diffusion of HCO produced by HCHO photodissociation in pressures of up to 250 Torr of Ar. Despite representation by the upper limit of k_d, diffusion plays little role in computed [HCO] decays which are governed by reaction losses. The initial concentrations of reactants ([HCHO] = 3.3×10^{16} molecule cm^{-3}, [Cl_2] = 0.9 to 2.7×10^{15} molecule cm^{-3}) and photoproducts ([HCO] and [H] of the order of $10^{13}-10^{14}$ molecule cm^{-3}, [Cl] $\approx 10^{13}$ molecule cm^{-3}) used in the model were deduced from experimental conditions and photochemical data of absorption cross-sections for HCHO and Cl_2 at a given wavelength. The initial conditions required $\Phi_{Cl} = 2$ for Cl_2 photolysis, and a value for Φ_{HCO}, which is what we seek experimentally. To determine absolute Φ_{HCO} values at the seven selected UV photolysis wavelengths, ACUCHEM model simulations using the data from Table 1 were carried out for HCHO/N_2 and HCHO/Cl_2/N_2 mixtures for each of the Cl_2 concentrations used in the experiments described in section 2.4. The computed data for the ratio $[HCO]_{tot}/[HCO]_{photo}$ at 10 μs (corresponding to the experimentally set delay between the photolysis and probe laser beams) were then plotted against [Cl_2]/[HCHO] and still displayed a linear relationship for [Cl_2] up to 2.3×10^{15} molecule cm^{-3}, despite the more complicated chemical model than that from which eq 9 was derived. By adjusting the value of Φ_{HCO} used to calculate the initial [HCO] input to the model, the gradient of a linear best fit to the simulated data plotted in the form of Figure 2 was matched quantitatively to the analogous best-fit gradient from the experimental data, thus yielding the absolute value of Φ_{HCO} for a given single photolysis wavelength.

Calculation of the initial [HCO] and [Cl] values also required knowledge of the volume of the photolysis laser beam. The diameter of this beam at the center of the ring-down chamber was measured as 0.9 mm, with a total length of 660 mm from the entrance to the exit windows of the chamber. This gave a total photolysis beam volume of 420 mm^3 (assuming a circular beam profile) with non-negligible measurement errors and additional associated uncertainty from the nonspatial-uniformity of the beam. The impact of the choice of photolysis laser volume on the Φ_{HCO} values was thus examined by running the complete kinetic model with initial inputs of [HCO] and [Cl] calculated using photolysis beam volumes taken to be equal to, and a factor of 2 greater and less than the measured beam volume. These simulations illustrated that the Φ_{HCO} values obtained by the data analysis using plots of the form shown in Figure 2 were insensitive to the UV beam volume, with changes of +1% and −4% for the larger and smaller volume respectively compared to use of the measured volume. Such small changes in Φ_{HCO} are within the quoted uncertainties (see section 3.2). This comparison serves to highlight that the dominant reactions occurring in the ring-down chamber are reactions 1, 2, 7, and 8 as described by eq 9, which results in an analysis procedure that is essentially independent of the photolysis laser beam volume. Thus by analyzing our data in the form plotted in Figure 2, i.e., as a ratio of the absorption coefficients (which are proportional to the concentrations) of HCO produced by HCHO photolysis only and in the presence of HCHO and Cl_2, we effectively eliminated the need for accurate determination of the photolysis beam volume.

Validation of the kinetic scheme of reactions 1, 2, 7, and 8 and Table 1 is important for the quantitative retrieval of Φ_{HCO} values. The scheme was therefore tested by comparing simulated time-dependent [HCO] decays to experimental measurements carried out by changing the time delay between the photolysis and probe laser beams in the range 0−80 μs. These time-dependent determinations of α_{HCO}^{rel} were undertaken for the photolysis of HCHO/N_2 and HCHO/Cl_2/N_2 mixtures, as described above. Measurements of α_{HCO}^{rel} were made at 5 μs delay

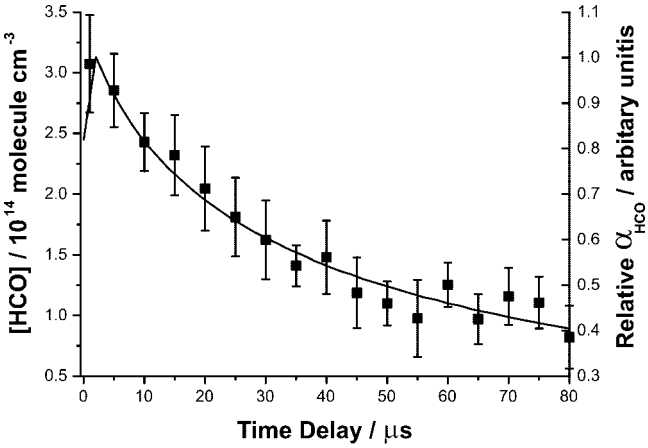

Figure 3. Experimentally measured [HCO] decay (■ and right-hand axis) with the time delay between the photolysis and probe lasers, and a simulation (— and left-hand axis) using the kinetic model outlined in Table 1, with integration using ACUCHEM for a representative mixture of HCHO + Cl_2. The initial rise in HCO at early times is a result of production via reaction of Cl atoms with HCHO.

intervals, with randomly alternated laser delays. Figure 3 shows a representative measured [HCO] decay for a HCHO/Cl_2/N_2 mixture, together with an ACUCHEM simulation. The specified HCO concentrations are the output from the kinetic simulation initiated with experimental conditions of [HCHO] = 3.3×10^{16} molecule cm^{-3} and [Cl_2] = 1.8×10^{15} molecule cm^{-3}, at a photolysis wavelength of 314.51 nm. The right-hand axis corresponds to the experimental relative absorption coefficient measurements (~5 measurements per data point), expressed in arbitrary units. The good agreement between the experimental and simulated rates of decay of HCO radicals shown in Figure 3 (and observed in other such data sets) confirms that the secondary chemistry occurring in the ring-down chamber is well described by the kinetic model of Table 1, and that estimates of the initial concentrations of HCO and Cl in the model are reliable. Inaccurate calculations of initial photoproduct concentrations would lead to a pronounced disagreement between the simulated and the experimental HCO decays. Additional measurements of HCO decays were carried out at different photolysis wavelengths and required different initial model input parameters (in accord with changes in absorption cross sections and quantum yields). These data were also accurately reproduced by the model, providing further evidence for the robust nature of this method for determining the final $\Phi_{HCO}(\lambda)$ values.

Typical RDTs for our apparatus under conditions of measurement of HCO absorption were, as noted in the preceding section, typically ~9−11 μs and could potentially introduce uncertainty in the measured time-dependence of α^{rel}_{HCO} data because of changes in [HCO] on comparable time scales. HCO absorption data shown in Figure 3 extending to 80 μs delays should, however, be largely unaffected by the time-averaging introduced by the CRDS measurements. The ring-down decays might also be affected by fast variations in [HCO], leading to nonsingle-exponential decay behavior and thus systematic errors in the retrieval of α^{rel}_{HCO} values. For reasons outlined below and from analysis of all sources of uncertainty in our data (see section 3.2), we conclude that these errors will be smaller than other sources of uncertainty identified in the derivation of relative and absolute HCO quantum yields.

The experimentally measured time dependencies of α^{rel}_{HCO} illustrated in Figure 3, and contained in other, similar data sets taken under different conditions, match the simulated [HCO] decays to within the uncertainties of all experimental data points over the relatively long time period from 0 to 80 μs. Any systematic errors in retrieval of HCO yields resulting from the effects described above must therefore be relatively minor. Moreover, these systematic errors will be smaller for the relative and absolute quantum yield data than for the kinetic data displayed in Figure 3, because the former were mostly obtained by using weaker HCHO absorption features and thus lower HCO radical number densities and second order loss rates. Analysis of kinetic data demonstrates that, over the characteristic time scales of the ring-down measurements (1 ring-down time interval initiated 10 μs after the photolysis laser pulse) the HCO concentrations change by <20%. Any uncertainties introduced from fitting of resultant nonsingle-exponential RD decays to a single-exponential model are incorporated in the errors in derived RDTs and are propagated into values of photochemical parameters as described in section 3.2. The uncertainties obtained from fitting decay traces in the presence of HCO radicals were no larger than those for analysis of the background ring-down decays (representative numbers for 1 SD uncertainties from the fits are 0.083 and 0.086 μs for ring-down traces obtained, respectively, with only a background of N_2 and in the presence of typical concentrations of HCO radicals), suggesting that deviations from single-exponential decays caused by reactive production and loss of HCO were not significant. All these arguments support the expectation that the measurements of α^{rel}_{HCO} are not systematically in significant error as a consequence of the ring-down measurement method.

3. Results and Discussion

3.1. Absolute HCO Quantum Yields. Absolute HCO quantum yields were measured at seven different tropospherically relevant HCHO photolysis wavelengths between 300 and 330 nm and are shown in Table 2. The lower limit for the wavelength resolution of these Φ_{HCO} data is estimated as ±0.005 nm, corresponding to the accuracy of the reported wavelength measurement and not limited by the laser bandwidth. Figure 4 shows the Φ_{HCO} measurements from the current work compared to those of Smith et al.[18] and the most recent recommendations of Sander et al.[1] All three Φ_{HCO} data sets display the same general trend with Φ_{HCO} values of ~0.6 ± 0.1 between 300 and 322 nm after which the values steadily decline. The three single wavelength Φ_{HCO} measurements between 303 and 309 nm from this work are significantly lower than both the current recommendations of Sander et al.[1] and the measurements of Smith et al.,[18] although in the latter case the data sets display overlapping error bars. Both of the single-wavelength Φ_{HCO} data sets display more wavelength variability than the current recommendations of Sander et al.[1]

It is important to stress that there are two significant differences between the Φ_{HCO} data set derived from the current work and that of Smith et al.[18] First, the latter Φ_{HCO} values were obtained from relative measurements scaled to a single reference wavelength value of 0.753 at 303.75 nm taken from DeMore et al.,[26] who recommended Φ_{HCO} values which were large and constant with wavelength. The data reported from the current study are, by contrast, independently measured absolute Φ_{HCO} values. Second, the resolution bandwidth of the spectrometer used by Smith et al.[18] (±0.62 nm) to measure relative HCO yields and the σ_{HCHO} values required to calculate Φ^{rel}_{HCO} was significantly larger than the Doppler width (0.0007 nm) of individual rotational features in the HCHO spectrum.[22] Earlier studies in our laboratory illustrated that spectrometer resolutions approaching the HCHO Doppler width are necessary to capture

TABLE 2: Absolute Φ_{HCO} and Uncertainty Data for HCHO Photolysis Measured at 294 K and under 100−200 Torr of N_2 Bath Gas[a]

λ/nm	gradient	r^2	ave $\sigma_{HCHO}/10^{-20}$ cm^2 molecule^{-1}	Φ_{HCO}	precision	uncertainty
303.70	8.8 ± 1.2	0.966	10.8 ± 2.6	0.62	0.03	0.09
306.13	14.3 ± 0.4	0.999	4.9 ± 0.2	0.57	0.03	0.10
308.78	14.4 ± 0.7	0.993	5.24 ± 0.17	0.61	0.07	0.08
314.31	10.9 ± 0.5	0.997	7.9 ± 1.5	0.69	0.04	0.06
320.67	27.3 ± 1.0	0.997	2.64 ± 0.15	0.64	0.02	0.10
325.59	27.7 ± 2.4	0.981	7.0 ± 1.6	0.51	0.04	0.10
329.51	22.8 ± 1.7	0.987	8.77 ± 0.66	0.28	0.09	0.11

[a] The columns are single wavelength data for the gradient (with 1 SD uncertainty) and correlation coefficients of the linear fits of the calibration plots of the type shown in Figure 2; HCHO absorption cross-sections averaged over ±0.005 nm of the measured wavelength (with 1 SD uncertainty); measured absolute HCO quantum yields, Φ_{HCO}; precision (1 SD) of Φ_{HCO} measurements derived from the errors on the gradients of the linear fits of the type shown in Figure 2; total uncertainty (1 SD) in Φ_{HCO} derived from the combined precision and uncertainty in the measured σ_{HCHO} (see text for further details).

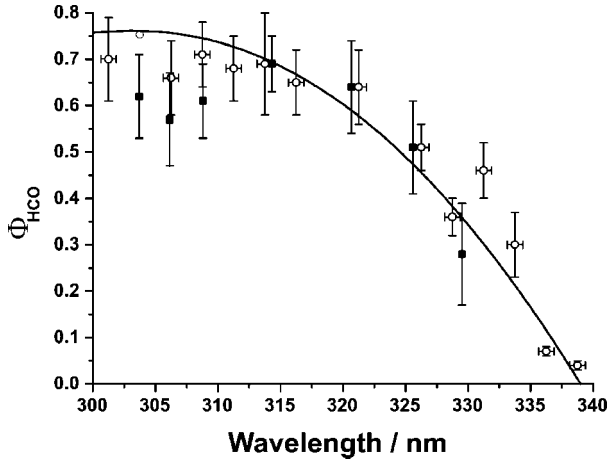

Figure 4. HCO quantum yield measurements, Φ_{HCO}: from this work (■), for $T = 294$ K and with 100−200 Torr N_2 bath gas; from Smith et al.[18] (○); and from the current recommendations of Sander et al.[1] (—). Vertical error bars for the current work represent ±1 SD measurement uncertainty (see Table 2) whereas those for the Smith et al.[18] data represent the 95% confidence limits. The spectral resolution of the measurements reported in this work was ±0.0035 nm and that of Smith et al.[18] was ±0.62 nm (represented as horizontal error bars). The data point of Smith et al.[18] at 303.75 nm is a calibration value[26] used to scale the remainder of their data, and is therefore plotted without error bars.

the significant rotational structure of the HCHO absorption spectra in the 300− 340 nm region, without which the absorption cross-sections at the peaks of the rovibrationally structured bands are underestimated.[20−22]As a result the Φ_{HCO} data of Smith et al.[18] may contain a non-negligible implicit inaccuracy derived from the wavelength averaged measurements of σ_{HCHO} used to calculate Φ^{rel}_{HCO}.

3.2. Uncertainty in Φ_{HCO}. Careful treatment of the uncertainties in the Φ_{HCO} values reported in this work is necessary for subsequent use in atmospheric models. Uncertainties are quoted throughout as 1 standard deviation (SD), derived from several steps in our procedure, and were quantified as follows. The first step in the data treatment was calculation of the precision in the individual $\alpha^{rel}_{HCO}(tot)/\alpha^{rel}_{HCO}(photo)$ measurements at a specific $[Cl_2]$ for a single wavelength. This precision was obtained by using the standard deviation in the RDT for each 50 data point measurement set and the signal from the photodiode measuring the UV light intensity prior to the chamber. The fractional errors in the measured $\alpha^{rel}_{HCO}(tot)/\alpha^{rel}_{HCO}(photo)$ ratios were typically between 10% and 30%. The major contribution to the uncertainty in $\alpha^{rel}_{HCO}(tot)/\alpha^{rel}_{HCO}(photo)$ resulted from the variability in the RDT on a shot-to-shot basis; amplitude noise on individual decay traces should have a negligible effect. Fitting what may be nonsingle-exponential decay traces (as discussed in section 2.5) to a single exponential decay model would also contribute to these fractional errors. Only a small (2−3%) uncertainty derives from the variability in the UV laser power. The precisions in the individual $\alpha^{rel}_{HCO}(tot)/\alpha^{rel}_{HCO}(photo)$ measurements were then used to calculate the weighted mean of 10−15 such ratios and its uncertainty for each data point corresponding to a particular $[Cl_2]/[HCHO]$ ratio.[43] The weighted means of $\alpha^{rel}_{HCO}(tot)/\alpha^{rel}_{HCO}(photo)$ were plotted versus $[Cl_2]/[HCHO]$ for each single wavelength Φ_{HCO} calibration point, and the linear regression was weighted by the uncertainties (see Figure 2). In this manner the variability in the measured RDT and the UV laser power, and therefore α^{rel}_{HCO}, were implicitly incorporated into the gradient (and its uncertainty) of the fits to the calibration plots. The precision on each of the single wavelength Φ_{HCO} measurements was then determined by using the chemical kinetic model and the range of the gradient of each calibration plot bounded by its uncertainties (3−14%) to determine the upper and lower limits for Φ_{HCO}. This precision is better than the uncertainties in the individual $\alpha^{rel}_{HCO}(tot)/\alpha^{rel}_{HCO}(photo)$ ratios because of the extensive averaging of data points and use of weighted linear regression in the procedures employed to obtain Φ_{HCO} values.

In the current study, the largest uncertainty in Φ_{HCO} derives from the highly structured bands of the HCHO absorption spectrum. The measured $\alpha^{rel}_{HCO}(photo)$ and $\alpha^{rel}_{HCO}(tot)$ were dependent on the absorption cross-section at the excitation wavelength, and the choice of value of σ_{HCHO} strongly influenced the initial conditions of the model, with direct impact upon derived Φ_{HCO} values. As described in section 2.4, high-resolution measurements of σ_{HCHO} (spectral resolution ±0.0035 nm) allowed the selection of relatively broad (>0.5 cm^{-1}) absorption bands for the reported single wavelength Φ_{HCO} measurements. This procedure minimized any uncertainty in subsequent analysis caused by small drifts in the UV photolysis laser frequency. HCHO absorption cross-sections used in the kinetic model to calculate the initial [HCO] values were the average over ±0.005 nm about the experimental fixed wavelengths (as specified in Table 2), which is the reported accuracy of the wavelength measurements. The variability in the average σ_{HCHO} is incorporated into the calibration plots of the type shown in Figure 2, where reduced correlation coefficients, and hence larger associated uncertainties in the gradients, were observed when Φ_{HCO} measurements were made on narrower HCHO absorption bands (see Table 2). The best estimates of the uncertainties in Φ_{HCO} are taken from combining the precision in Φ_{HCO} with the reported measurement uncertainties in the σ_{HCHO} values which range between 5% and 10%[22] depending on the HCHO

absorption band upon which the measurements were made. This led to total estimated absolute uncertainties in the measured Φ_{HCO} of magnitudes between 0.06 and 0.11, as listed in the final column of Table 2.

An additional potential source of error in the Φ_{HCO} measurements derives from the uncertainties in the rate constants used in the kinetic model (see Table 1 and section 2.5). A sensitivity study of the model to the individual rate constant uncertainties determined that the impact upon the gradient of simulated [HCO](tot)/[HCO](photo) versus $[Cl_2]$/[HCHO] plots was a reduction of 7% for $k_{HCO+HCO}$, and increases of 6% for k_{HCO+H} and 3% for k_{H+Cl_2} for cases in which the positive uncertainty on each of the rate constants was used. The impact on the gradient of the remaining rate constant uncertainties was <1%. On the basis of these results, and also the good agreement between the experimental and simulated HCO decay in the presence of HCHO + Cl_2 (see Figure 3), the uncertainties in the rate constant used in the kinetic model were not considered to impact significantly upon the total uncertainty in Φ_{HCO}.

3.3. Bath Gas Pressure Dependence of Φ_{HCO}. All of the σ_{HCHO}, α_{HCO}^{rel}, and Φ_{HCO} measurements reported in this and our earlier work[20−22] were carried out in 100−200 Torr of N_2 bath gas with the main purpose of thermalizing vibrationally and rotationally excited HCO radicals to allow quantitative detection by CRDS as described in section 2.4. The effects of bath gas pressure on the Φ_{HCO} measurements must, however, be addressed because quenching of the $\tilde{A}^1A_2$ (S_1) singlet excited state of HCHO may affect HCO yields. Moortgat and Warneck[14] previously reported that addition of up to 800 Torr of air did not influence the HCO yields in the 290−330 nm wavelength range. The reasons for this lack of perturbation in the photochemical processes by addition of different pressures of bath gas are suggested to be 2-fold. First, the lifetimes of the vibrational levels of the S_1 electronic state of HCHO are short (in the range of a few nanoseconds for the upper state levels of the 2^14^3 and 2^24^1 bands) and decrease with increasing vibrational excitation.[44] Second, N_2 is a nonpolar molecule with a singlet ground state, and thus, it is not an effective collision partner for electronic quenching processes.[44,45] Experimental test measurements of α_{HCO}^{rel} at different pressures (up to 500 Torr of N_2) carried out in our laboratory at UV wavelengths between 320 and 332 nm, where all of the nascent HCO photoproduct is expected to be in its vibrational ground state, also showed no pressure dependence on HCO yields, as exemplified in Figure 1 by data taken with 0 and 200 Torr of N_2 bath gas. The HCO yield values reported herein, taken under conditions of 200 Torr of N_2, are thus not thought to be influenced by the presence of the bath gas, and are appropriate for use in models for up to 1 atm of air. However, we note that we were unable to test the effect of O_2 on Φ_{HCO} values because rapid reaction of HCO radicals with added O_2 would remove our source of signal for the measurements.

3.4. Data for Atmospheric Modeling. The products of HCO quantum yield and HCHO absorption cross-section values, $\Phi_{HCO}\sigma_{HCHO}$, at wavelengths between 302.6 and 331.0 nm at a temperature of 294 K and under 200 Torr of N_2 bath gas are presented in Figure 5 with the data binned into 0.1 nm wavelength intervals. This product of Φ_{HCO} and σ_{HCHO} is the most appropriate representation of the accumulation of data from our studies of HCHO photochemistry because it can be used directly with solar flux data to calculate J(HCO) (eq 3) for atmospheric models.

The $\Phi_{HCO}\sigma_{HCHO}$ product is directly proportional to the relative HCO absorption coefficient measurements, α_{HCO}^{rel} (eq 6) that arise from our experiments. Separation of the quantum yield and cross-section values would introduce significant noise and uncertainty into the data (particularly in regions of weak UV absorption), and is thus avoided, but $\sigma_{HCHO}(\lambda)$ values are separately available.[22] The α_{HCO}^{rel} measurements were thus independently scaled to give absolute values of the $\Phi_{HCO}\sigma_{HCHO}$ product using the seven measured single wavelength Φ_{HCO} calibration points and our high-resolution σ_{HCHO} values measured at the same wavelength and spectrometer resolution.[22] Single wavelength measurements of absolute Φ_{HCO} values were made for most of the major HCHO S_1-S_0 absorption bands to ensure that the scaling procedure was reliable and that α_{HCO}^{rel} values for each band were referenced independently to an absolute value. Although there is no single wavelength Φ_{HCO} calibration point measured for the 2^24^3 (316.4−318.5 nm) band, our spectra for HCO production in this region overlapped with the lower wavelength band at 313.5−315.6 nm. We note that the $\Phi_{HCO}\sigma_{HCHO}$ data presented are applicable at the total pressure at which they were measured, i.e. with 200 Torr of N_2; for higher pressures of bath gas, a minor correction will be necessary to account for the effect of pressure broadening on σ_{HCHO} values. The pressure broadening correction to linewidths was previously estimated to correspond to 0.2−0.3 cm^{-1} atm^{-1},[22] and results in a reduction in the σ_{HCHO} (and thus $\Phi_{HCO}\sigma_{HCHO}$) values at any particular wavelength.

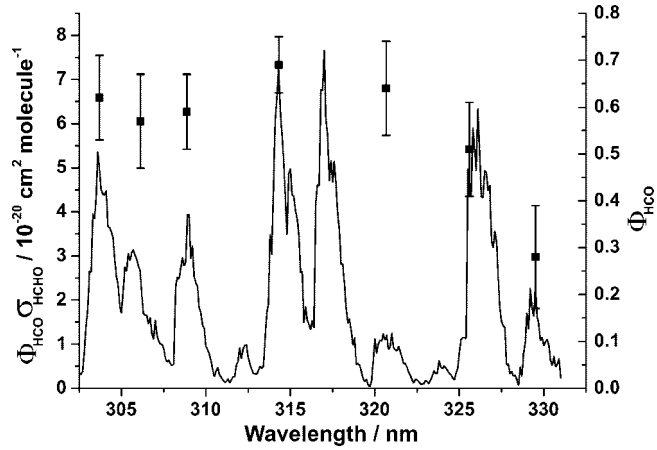

Figure 5. The product of the HCHO absorption cross-sections and HCO quantum yields ($\Phi_{HCO}\sigma_{HCHO}$) at $T = 294$ K and with 200 Torr of N_2, binned into 0.1 nm wavelength intervals (—). Wavelength-dependent HCO absorption coefficients were scaled by using single wavelength Φ_{HCO} data (■, right-hand axis) and measured σ_{HCHO} values to give the plotted data. Vertical error bars on the single wavelength Φ_{HCO} data represent ±1 SD uncertainties in the measurements. In regions where HCO absorption coefficients were not measured (306.9−308.6, 310.5−313.3, 319.2−325.2, 327.6−328.7 nm) $\Phi_{HCO}\sigma_{HCHO}$ values were estimated by interpolating the single wavelength Φ_{HCO} data, as described in the text.

The $\Phi_{HCO}\sigma_{HCHO}$ data shown in Figure 5 for photolysis wavelength intervals 306.9−308.6, 310.5−313.3, 319.2−325.2 (5^1_0 band), and 327.6−328.7 nm represent wavelengths at which α_{HCO}^{rel} measurements were not carried out because of the limited signal-to-noise ratios obtained for $\sigma_{HCHO} < 1.8 \times 10^{-20}$ cm^2 $molecule^{-1}$. We were unable to increase the HCHO pressure to improve the signal levels because of the errors introduced into HCHO absorption cross-section values at partial pressures larger than 1 Torr.[13] To complete the data set, the missing $\Phi_{HCO}\sigma_{HCHO}$ data for these wavelength ranges were estimated by multiplying interpolated absolute Φ_{HCO} values by the corresponding experimental σ_{HCHO} data sets. The interpolation procedure for the small absorption band at 319−324 nm, which represents the largest

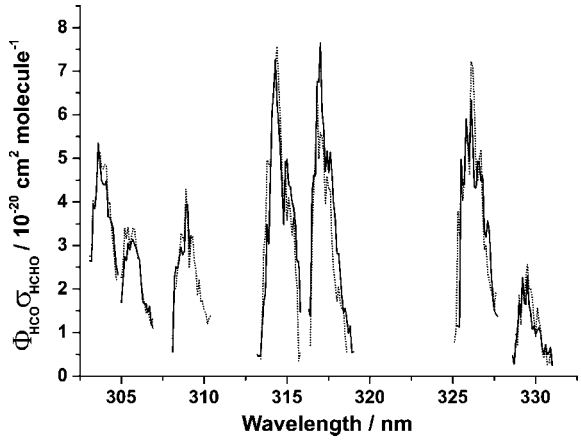

Figure 6. Wavelength-dependent $\Phi_{HCO}\sigma_{HCHO}$ values at 294 K (—) and 245 K (---) measured with 200 Torr of N_2 bath gas. The data are binned into 0.1 nm wavelength intervals. Gaps in the data set represent regions in which the instrument signal-to-noise was insufficient to measure relative HCO absorption coefficients, α_{HCO}^{rel}, because of low σ_{HCHO} values.

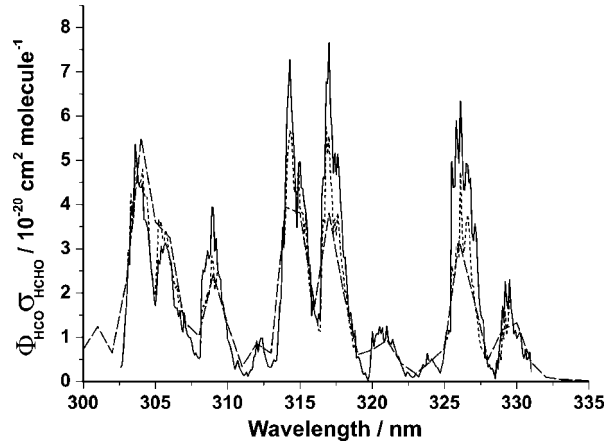

Figure 7. The 294 K data from Figure 6 (—) are compared with (incorrect) $\Phi_{HCO}\sigma_{HCHO}$ values derived by simple linear interpolation of quantum yields between the single-wavelength Φ_{HCO} measurements shown in Figure 4 (---). The plot also shows values of $\Phi_{HCO}(\lambda)\sigma_{HCHO}(\lambda)$ calculated by using the current recommendations of Sander et al.[1] (— — —) with a best wavelength resolution of 1 nm.

gap in the $\Phi_{HCO}\sigma_{HCHO}$ data set, was considered to be reliable because a single wavelength Φ_{HCO} calibration point was measured at 320.14 nm. There were also an additional 31 $\Phi_{HCO}\sigma_{HCHO}$ data points (for $T = 294$ K), mainly on the edges of absorption bands, for which further interpolation or an alternative minor correction was made because of apparent inaccuracies in the data, and the correction procedure used is explained in the Supporting Information. Analysis of the uncertainties in the $\Phi_{HCO}\sigma_{HCHO}$ data sets suggests that a 15% (1 SD) precision is appropriate for applications that incorporate the entire wavelength range in calculations of photochemical rate coefficients. If, however, $\Phi_{HCO}\sigma_{HCHO}$ data spanning smaller portions of the spectrum are to be used, the following uncertainties apply to the individual vibronic bands: 15% (302−305 nm; $2_0^4 4_0^1$ band); 19% (305−308 nm; $2_0^3 4_0^3$ band); 11% (308−310 nm; $2_0^1 5_0^1$ band); 11% (310−313 nm, weak bands); 8% (313−316 nm; $2_0^3 4_0^1$ band); 10% (316−320 nm; $2_0^2 4_0^3$ band); 17% (320−325 nm; 5_0^1 and weak bands); 15% (325−328 nm; $2_0^2 4_0^1$ band); and 32% (328−331 nm; $2_0^1 4_0^3$ band).

Figure 6 illustrates the effect on $\Phi_{HCO}\sigma_{HCHO}$ of reducing the temperature within the ring-down chamber from 294 to 245 K, using the coolant circulation system described in section 2.1. Simultaneous measurements of σ_{HCHO} and α_{HCO}^{rel} were made for the 300−332 nm spectral range. Single wavelength Φ_{HCO} calibration points were not, however, measured at low temperature, and thus relative α_{HCO}^{rel} values at 245 K were scaled by using Φ_{HCO} data measured at 294 K and σ_{HCHO} measured at 245 K. The assumption that temperature does not affect Φ_{HCO} values for wavelengths between 300 and 330 nm is supported by our measurements of α_{HCO}^{rel} at 245 K, which showed minimal difference to those measured at 294 K (within the uncertainties of the data sets).[32] The findings of Moortgat et al.[15] reinforce this assumption. At the high wavelength resolution of our experiment, HCHO molecules are excited only to a small number of rovibrational levels of the S_1 state when the laser is tuned to a single absorption feature. There is no reason to suppose that the couplings from the S_1 state to the T_1 or S_0 states, via which dissociation through channels 1 or 2 occur, are strongly temperature dependent. Collisional quenching or collision-induced couplings to T_1 or S_0 might be temperature dependent, but are not thought to be significant relaxation mechanisms.

Vibrational partition functions at 294 and 245 K were calculated using the six normal vibrational modes of HCHO in its ground electronic state, by approximating them as harmonic oscillators. These calculations confirmed that the number of states thermally accessible to HCHO were very similar (the partition functions agree to within 0.5%) for the two temperatures. This calculation suggests that the integrated band intensities for individual rovibronic bands of the HCHO absorption spectra should be essentially independent of temperature over the range 245−294 K. The measured HCHO absorption cross-sections were integrated for each of the major vibronic bands in the 300−335 nm wavelength range, and the integrated intensities were found to be very similar at both temperatures (the maximum difference was 7% of the total band strength for the $2_0^3 4_0^3$ vibronic band),[22] in accord with the expectations of the vibrational partition function calculations. The more significant effect of temperature changes is to redistribute absorption intensity within the bands through changing population of rotational levels, which can be modeled with spectral simulation programs such as PGOPHER[46] for which simulation files are available.[22] As Figure 6 shows, with our assumption of Φ_{HCO} being independent of temperature, the temperature effects on the $\sigma_{HCHO}(\lambda)$ did not cause a significant impact upon the $\Phi_{HCO}\sigma_{HCHO}$ product. The small differences in wavelength-dependent $\Phi_{HCO}\sigma_{HCHO}$ values at 294 and 245 K do not illustrate a particular trend and are within the combined uncertainties associated with the α_{HCO}^{rel}, Φ_{HCO}, and σ_{HCHO} measurements.

A comparison between the wavelength dependence of the $\Phi_{HCO}\sigma_{HCHO}$ product from this work and that calculated by using the recommendations of Sander et al.[1] is displayed in Figure 7. Significant discrepancies are clear, especially in the 312−318 and 325−329 nm ranges in which $\Phi_{HCO}\sigma_{HCHO}$ values from this work approach double those recommended in the NASA-JPL compilation.[1] These discrepancies, in the most part, result from the lower resolution of the spectrometers used to measure the Φ_{HCO} and σ_{HCHO} data upon which the recommendations of Sander et al.[1] are based.

It is important to note that calculation of a $\Phi_{HCO}\sigma_{HCHO}$ data set by interpolation of our single wavelength Φ_{HCO} values followed by multiplication by the σ_{HCHO} data from this laboratory[20−22] at the same wavelength resolution results in incorrect $\Phi_{HCO}\sigma_{HCHO}$ values, as is also illustrated in Figure 7. The $\Phi_{HCO}\sigma_{HCHO}$ data produced using the interpolation of single-

wavelength Φ_{HCO} data are up to a factor of 2 smaller than those obtained by the chosen method of scaling our α_{HCO}^{rel} measurements using σ_{HCHO} and Φ_{HCO} data described earlier in this section. The reduced $\Phi_{HCO}\sigma_{HCHO}$ values resulting from the interpolation procedure are a consequence of neglect of the significant wavelength-dependent variability in Φ_{HCO} values, which goes beyond that captured in the seven single wavelength values reported here. By using our previously measured high wavelength resolution α_{HCO}^{rel} and σ_{HCHO}[20−22] data to create a complete $\Phi_{HCO}(\lambda)\sigma_{HCHO}(\lambda)$ data set from the single wavelength Φ_{HCO} measurements, we incorporate the effects of the wavelength variability in Φ_{HCO} and thus derive higher $\Phi_{HCO}\sigma_{HCHO}$ values. The effects of the interpolation procedure are particularly important at the maxima of the $2_0^3 4_0^1$, $2_0^2 4_0^3$, and $2_0^2 4_0^1$ HCHO absorption bands, which impact significantly upon the calculated J(HCO).

No significant pressure or temperature dependence of HCO yields was observed for the wavelength range of this study. As a result, a total quantum yield of unity for photoproducts from channels 1 and 2 of HCHO photolysis for this wavelength range is indicated, i.e., $\Phi_{H_2} + \Phi_{HCO} = 1$, in accord with the work of Moortgat and Warneck.[14] The assumption of a negligible fluorescence quantum yield (Φ_f) borne out by previously reported zero-pressure values of $\Phi_f = 0.033$ for the low-energy 4^1 rovibronic band ($\lambda \approx 353$ nm),[47,48] and a rapid decrease of radiative lifetimes of the vibronic bands with increasing excitation energy, reinforce the assertion that $\Phi_{H_2} + \Phi_{HCO} = 1$.[44] On the basis of such an assumption, and for the purposes of atmospheric modeling, data sets for the wavelength-dependent product of the HCHO absorption cross-section and the quantum yields for the molecular channel, eq 1 $\Phi_{H_2}\sigma_{HCHO}$, at 294 and 245 K and for 200 Torr of N_2 bath gas were produced by using

$$\Phi_{H_2}\sigma_{HCHO} = \sigma_{HCHO} - \Phi_{HCO}\sigma_{HCHO} \quad (10)$$

These data are provided in the Supporting Information at 0.1 and 1.0 nm wavelength resolution. An explanation of minor corrections to the data is also provided in the Supporting Information.

3.5. Atmospheric Implications. In the 300−330 nm region, the differences between the current $\Phi_{HCO}\sigma_{HCHO}$ data and those recommended by Sander et al.[1] have the potential to impact significantly upon calculated HO_x production rates from HCHO photolysis because of the abrupt change in the solar photon flux with wavelength. To account properly for the wavelength-dependent photolysis of HCHO, we recommend the use of data measured at high spectral resolution, which can be carefully binned to give lower wavelength resolution data sets for computational expediency, in order to reproduce correctly the impact of HCHO photolysis on tropospheric chemistry.

The NCAR Tropospheric Ultraviolet and Visible (TUV) radiation model[49] was used to produce a high-wavelength resolution (0.1 nm) data set for the solar photon flux. These data were used along with our new data for the product $\Phi_{HCO}\sigma_{HCHO}$ to produce a data set for the wavelength-dependent HCHO photolysis rate coefficients for the radical channel, J(HCO,λ) (eq 3), at solar zenith angles of 0°, 40°, 60°, 70°, and 80°. By integrating the J(HCO,λ) values over the range λ = 302.6 to 331.0 nm (eq 3), J(HCO) = 4.67×10^{-5} s^{-1} is obtained for solar photon flux data at ground level at midday on 30th June and 50° north. The calculated J(HCO, λ) were also binned to reduce the wavelength resolution to 1.0 nm, integrated between λ = 303 and 330 nm and compared to J(HCO) values calculated with the current NASA-JPL recommendations for quantum yields and cross-sections,[1] which are provided with a best resolution of 1.0 nm. A plot of our calculated J(HCO) values for five SZAs relative to those calculated using the current NASA-JPL recommendations is shown in Figure 8. The net increase in calculated J(HCO) on application of our new data for the product $\Phi_{HCO}\sigma_{HCHO}$ is 25% for SZA of 0°, increasing monotonically to 33% for SZA of 80°. The uncertainties in our calculated J(HCO) are estimated to be ±15% using the average uncertainty in the single wavelength Φ_{HCO} values, and assuming much smaller contributions from the measured α_{HCO}^{rel} and σ_{HCHO} values, and the solar photon flux data. No estimation of the uncertainty in the Φ_{HCO} and σ_{HCHO} values is provided in the NASA-JPL recommendations.[1] The new J(HCO) data are comparable to those of Smith et al.,[18] who reported net increases in J(HCO) compared to the recommendations of DeMore et al.[26] ranging from 8% to 21% as SZA increased.

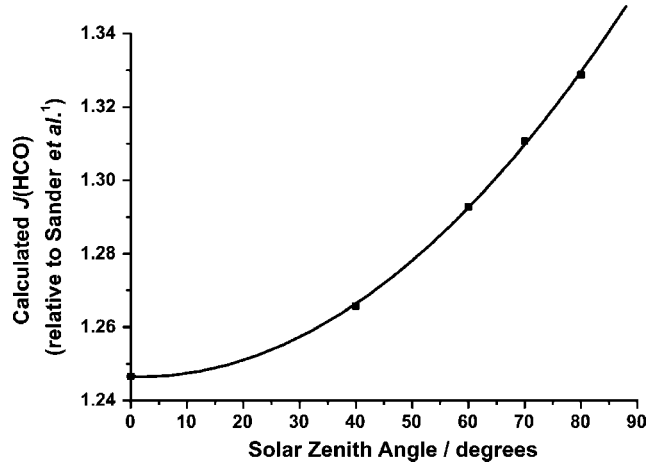

Figure 8. HCHO photolysis frequencies for the radical channel, J(HCO) calculated from the photochemical data from this work are compared as a ratio with the J(HCO) values calculated with the same wavelength-dependent solar flux data, but using the recommendations for absorption cross-sections and quantum yields of Sander et al.[1] The ratios are presented as a function of solar zenith angle. Calculated J(HCO) values from this work have an estimated ±15% error.

4. Conclusions

Absolute quantum yields for the H + HCO production from HCHO photodissociation (Φ_{HCO}) have been determined at seven UV wavelengths. The measurements employed direct detection of HCO radicals by CRDS, and compared photolytic yields of HCO with those from the reaction of HCHO with Cl atoms produced from Cl_2 photolysis. The absolute Φ_{HCO} values were used to scale an extensive set of relative HCO absorption coefficients, α_{HCO}^{rel}, measured at very high wavelength resolution, to provide a complete data set of $\Phi_{HCO}(\lambda) \times \sigma_{HCHO}(\lambda)$ data for formaldehyde photolysis in the tropospherically important wavelength range from 302 to 331 nm. No significant pressure or temperature dependence of the HCO yield was observed, consistent with a total quantum yield of unity for photoproducts from the radical (H + HCO) and molecular (H_2 + CO) channels. With the assumption that $\Phi_{H_2} + \Phi_{HCO} = 1$, values of $\Phi_{H_2}(\lambda) \times \sigma_{HCHO}(\lambda)$ were derived over the same wavelength range.

The set of wavelength-dependent products of absorption cross-sections and radical quantum yields was combined with high-resolution solar photon flux data to calculate J(HCO,λ), the integrated photolysis rate constants for HCHO photodissociation via the radical channel, at different SZAs. Comparison with the latest NASA-JPL recommendation suggests an increased J(HCO) of 25% at 0° SZA increasing to 33% at high

SZA (80°), which is likely to impact significantly upon calculated HO_x production rates from HCHO photolysis in atmospheric models.

The current study highlights the importance of using high-resolution spectroscopic techniques to achieve a complete and accurate picture of HCHO photodissociation processes. Data measured with lower resolution spectrometers lead to underestimation of the photochemical role of such species in tropospheric chemistry because of their complicated dissociation dynamics and highly structured spectroscopy. Wavelength-dependent data for the product of the absolute radical quantum yield and HCHO absorption cross-section, $\Phi_{HCO}\sigma_{HCHO}$, at 294 and 245 K and with 200 Torr of N_2 bath gas between 302.6 and 331.0 nm are available as Supporting Information with wavelength resolutions of 0.005, 0.1, and 1.0 nm. The products of the molecular channel quantum yields and HCHO absorption cross-sections, $\Phi_{H_2}\sigma_{HCHO}$, are also provided for the same experimental conditions at 0.1 and 1.0 nm wavelength resolution.

Acknowledgment. Funding for equipment and for SCS and ALH from NERC grant NE/D001498/1 is gratefully acknowledged, along with support for PGC from the EU Marie Curie Early Stage Training grant BREATHE (MEST-CT-2004-514499). We thank A.T. Archibald for providing high-resolution solar photon flux data. A.J.O.E. thanks the Royal Society and Wolfson Foundation for a Research Merit Award.

Supporting Information Available: Tabulated numerical data for the wavelength-dependence of the product of the HCO radical quantum yield (Φ_{HCO}) from HCHO photolysis and HCHO absorption cross-section, σ_{HCHO}, measured at 294 and 245 K in the presence of 200 Torr of N_2 bath gas (the 245 K data were calculated using α_{HCO}^{rel} and σ_{HCHO} measurements at 245 K, but scaled with absolute Φ_{HCO} values for $T = 294$ K); all data for wavelengths from 302.6 to 331.0 nm, with resolutions of 0.005, 0.1, and 1.0 nm; the derived products of the molecular ($H_2 + CO$) quantum yield and HCHO absorption cross-sections, $\Phi_{H_2}\sigma_{HCHO}$, at $T = 294$ and 245 K and with 200 Torr of N_2 bath gas at 0.1 and 1.0 nm wavelength resolution between 302.6 and 331.0 nm, which are valid if $\Phi_{H_2} + \Phi_{HCO} = 1$. This material is available free of charge via the Internet at http://pubs.acs.org.

References and Notes

(1) Sander, S. P.; Golden, D. M.; Kurylo, M. J.; Moorgat, G. K.; Wine, P. H.; Ravishankara, A. R.; Kolb, C. E.; Molina, M. J.; Finlayson-Pitts, B. J.; Huie, R. E.; Orkin, V. L. *NASA JPL Publ.* **2006**, *06-2*.

(2) Zhou, X.; Mopper, K.; Lee, Y.-N.; Newman, L.; Chen, X. *J. Geophys. Res* **1996**, *101*, 14711.

(3) Williams, I. D.; Revitt, D. M.; Hamilton, R. S. *Sci. Total Environ.* **1996**, *190*, 475.

(4) Garcia, A. R.; Volkamer, R.; Molina, L. T.; Molina, M. J.; Samuelson, J.; Mellqvist, J.; Galle, B.; Herndon, S. C.; Kolb, C. E. *Atmos. Chem. Phys.* **2006**, *6*, 4545.

(5) Valachovic, L. R.; Tuchler, M. F.; Dulligan, M.; Droz-Georget, T.; Zyrianov, M.; Kolessov, A.; Reisler, H.; Wittig, C. *J. Chem. Phys.* **2000**, *112*, 2752.

(6) Smith, S. C.; Lee, J. D.; Bloss, W. J.; Johnson, G. P.; Ingham, T.; Heard, D. E. *Atmos. Chem. Phys.* **2006**, *6*, 1435.

(7) Holland, F.; Hofzumahaus, A.; Schafer, R.; Kraus, A.; Patz, H. W. *J. Geophys. Res.* **2003**, *108*, 8246.

(8) Martinez, M.; Harder, H.; Kovacs, T. A.; Simpas, J. B.; Bassis, J.; Lesher, R.; Brune, W. H.; Frost, G. J.; Williams, E. J.; Stroud, C. A.; Jobson, B. T.; Roberts, J. M.; Hall, S. R.; Shetter, R. E.; Wert, B.; Fried, A.; Alicke, B.; Stutz, J.; Young, V. L.; White, A. B.; Zamora, R. J. *J. Geophys. Res.* **2003**, *108*, 4617.

(9) Lewis, R. S.; Tang, K. Y.; Lee, E. K. C. *J. Chem. Phys.* **1976**, *65*, 2910.

(10) Marling, J. *J. Chem. Phys.* **1977**, *66*, 4200.

(11) Horowitz, A.; Calvert, J. G. *Int. J. Chem. Kinet.* **1978**, *10*, 805.

(12) Clark, J. H.; Moore, C. B.; Nogar, N. S. *J. Chem. Phys.* **1978**, *68*, 1264.

(13) Tang, K. Y.; Fairchild, P. W.; Lee, E. K. C. *J. Phys. Chem.* **1979**, *83*, 569.

(14) Moortgat, G. K.; Warneck, P. *J. Chem. Phys.* **1979**, *70*, 3639.

(15) Moortgat, G. K.; Seiler, W.; Warneck, P. *J. Chem. Phys.* **1983**, *78*, 1185.

(16) Moore, C. B.; Weisshaar, J. C. *Annu. Rev. Phys. Chem.* **1983**, *34*, 525.

(17) Meller, R.; Moortgat, G. K. *J. Geophys. Res.* **2000**, *105*, 7089.

(18) Smith, G. D.; Molina, L. T.; Molina, M. J. *J. Phys. Chem. A* **2002**, *106*, 1233.

(19) Troe, J. *J. Phys. Chem. A* **2007**, *111*, 3862.

(20) Pope, F. D.; Smith, C. A.; Ashfold, M. N. R.; Orr-Ewing, A. J. *Phys. Chem. Chem. Phys.* **2005**, *7*, 79.

(21) Pope, F. D.; Smith, C. A.; Davis, P. R.; Shallcross, D. E.; Ashfold, M. N. R.; Orr-Ewing, A. J. *Faraday Discuss.* **2005**, *130*, 1.

(22) Smith, C. A.; Pope, F. D.; Cronin, B.; Parkes, C. B.; Orr-Ewing, A. J. *J. Phys. Chem. A* **2006**, *110*, 11645.

(23) Gratien, A.; Nilsson, E.; Doussin, J.-F.; Johnson, M. S.; Nielsen, C. J.; Stenstrom, Y.; Picquet-Varrault, B. *J. Phys. Chem. A* **2007**, *111*, 11506.

(24) Gratien, A.; Picquet-Varrault, B.; Orphal, J.; Perraudine, E.; Flaud, J.-F. *J. Geophys. Res.* **2007**, 112, X.

(25) Cantrell, C. A.; Davidson, J. A.; McDaniel, A. H.; Shetter, R. E.; Calvert, J. G. *J. Phys. Chem.* **1990**, *94*, 3902.

(26) DeMore, W. B.; Sander, S. P.; Golden, D. M.; Hampson, R. F.; Kurylo, M. J.; Howard, C. J.; Ravishankara, A. R.; Kolb, C. E.; Molina, M. J. *NASA JPL Publ.* **1997**, *97-4*.

(27) Spence, R.; Wild, W. *J. Chem. Soc.* **1935**, *1*, 338.

(28) Mazurenka, M.; Wada, R.; Shillings, A. J. L.; Butler, T. J. A.; Beames, J. M.; Orr-Ewing, A. J. *Appl. Phys. B: Laser Opt.* **2005**, *81*, 135.

(29) *LabView*, version 6; National Instruments, Austin, TX, 2000.

(30) Flad, J. E.; Brown, S. S.; Burkholder, J. B.; Stark, H.; Ravishankara, A. R. *Phys. Chem. Chem. Phys.* **2006**, *8*, 3636.

(31) Zalicki, P.; Zare, R. N. *J. Chem. Phys.* **1995**, *102*, 2708.

(32) Smith, C. A. The Atmospheric Photochemistry of Formaldehyde. Ph.D. thesis, University of Bristol, 2006.

(33) Mazurenka, M.; Orr-Ewing, A. J.; Peverall, R.; Ritchie, G. A. D. *Annu. Rep. C* **2005**, *101*, 100.

(34) Hopkins, W. S.; Loock, H. P.; Cronin, B.; Nix, M. G. D.; Devine, A. L.; Dixon, R. N.; Ashfold, M. N. R. *J. Chem. Phys.* **2007**, *127*, 064301.

(35) Chen, Y. Q.; Zhu, L. *J. Phys. Chem.* **2003**, *107*, 4643.

(36) Zhu, L.; Kellis, D.; Ding, C.-F. *Chem. Phys. Lett.* **1996**, *257*, 487.

(37) Wang, L. M. *Faraday Discuss.* **2005**, *130*, 125.

(38) Okabe, H. *Photochemistry of small molecules*; John Wiley & Sons, Inc.: New York, 1978.

(39) Maric, D. B. P.; Meller, R.; Moortgat, G. J. *Photochem. Photobiol.* **1993**, *70*, 205.

(40) Braun, W.; Herron, J. T.; Kahaner, D. K. *Int. J. Chem. Kinet.* **1988**, *20*, 51.

(41) Langford, O.; Moore, C. B. *J. Chem. Phys.* **1984**, *80*, 4204.

(42) Reilly, J. P.; Clark, J. H.; Moore, C. B.; Pimentel, G. C. *J. Chem. Phys.* **1978**, *69*, 4380.

(43) Bevington, P. R.; Robinson, K. *Data reduction and error analysis*, 3rd ed.; McGraw Hill: New York, 2002.

(44) Yeung, E. S.; Moore, C. B. *J. Chem. Phys.* **1973**, *58*, 3988.

(45) Weisshaar, J. C.; Bamford, D. J.; Specht, E.; Moore, C. B. *J. Chem. Phys.* **1981**, *74*, 226.

(46) Western, C. M. *PGOPHER - A program for simulating rotational structure*; University of Bristol, Bristol (http://pgopher.chm.bris.ac.uk).

(47) Fairchild, P. W.; Shibuya, K.; Lee, E. K. *J. Chem. Phys.* **1981**, *75*, 3407.

(48) Shibuya, K.; Fairchild, P. W.; Lee, E. K. *J. Chem. Phys.* **1981**, *75*, 3397.

(49) Madronich, S.; Flocke, S. *The role of solar radiation in atmospheric chemistry*; Springer-Verlag: Heidelberg, Germany, 1998.

(50) Poulet, G.; Laverdet, G.; Le Bras, G. *J. Chem. Phys.* **1984**, *80*, 1922.

(51) Baulch, D. L.; Cobos, C. J.; Cox, R. A.; Esser, C.; Frank, P.; Just, T.; Kerr, J. A.; Pilling, M. J.; Troe, J.; Walker, R. W.; Warnatz, J. *J. Phys. Chem. Ref. Data* **1992**, *21*, 411.

(52) Ninomiya, Y.; Goto, M.; Hashimoto, S.; Kagawa, Y.; Yoshizawa, K.; Kawasaki, M.; Wallington, T. J.; Hurley, M. D. *J. Phys. Chem. A* **2000**, *104*, 7556.

(53) Bemand, P. P.; Clyne, M. A. A. *J. Chem. Soc., Faraday Trans* **1977**, *73*, 394.

JP8070508